Supplementary Information

Ultra-durable Two-Electrode Zn-air Secondary Batteries Based on Bifunctional Titania Nanocatalysts: Co^{2+} Dopants Boosts the Electrochemical Activity

Li-Na Han, Li-Bing Lv, Qian-Cheng Zhu, Xiao Wei, Xin-Hao Li* and Jie-Sheng Chen*

Experimental Section

Electrocatalysts synthesis: All chemicals were analytical-grade reagents and used as purchased without further purification. The TiO_2 nanoparticles with various Co-doping contents were prepared by sol-gel method according to previous report with slight modification. TiO_2 nanoparticles were prepared with a precursor solution consisting of titanium tetraisopropoxide (TTIP), ethanol, hydrochloric acid (HCl), deionized water, Pluronic P123 (and a certain amount of $CoSO_4 \cdot 7H_2O$ was added to obtain Co-doped TiO_2 nanoparticles), with molar ratios of TTIP/P123/HCl/H_2O/ ethanol at 1:0.005:0.5:15:40. The solution was heated at 40 °C for 12 h and then dried at room temperature naturally. The dried powders were calcinated at 550 °C for 3 h to remove the organic and enhance the crystallization of TiO_2.

Characterizations: X-ray diffraction (XRD) patterns were obtained by X-ray diffraction (Rigaku D/Max-2550, Cu Ka$\square\lambda\square$= 1.54056 Å) measurement. SEM measurements were performed on a FEI Nova NanoSEM 2300. During imaging, the samples were kept at a distance of 5 mm from the electron source and the voltage was kept at 5 kV. No particular types of preparation were implemented before imaging. Transmission electron microscopy (TEM) and High-resolution transmission electron microscopy (HRTEM) measurements were taken with a JEM-2100 microscope operated at 200 kV accelerating voltage. X-ray photoemission spectroscopy (XPS) analyses were performed on a Kratos Axis Ultra DLD spectrometer with Al Kα radiation source. Invia-reflex micro-Raman spectrometer (Renishaw, UK) was used to detect the g-N-MM-Cnet and layered carbon with a 633 nm wavelength incident laser. A NOVA 2200e analyzer (Quntachrome, USA) was used to measure Brunauer-Emmett-Teller surface area. Samples were degassed at 200 °C for 12 h before measurements.

The X-ray absorption data at the Co K-edge of the samples were recorded at room temperature in transmission mode using ion chambers at beamline BL14W1 of the Shanghai Synchrotron Radiation Facility (SSRF). The station was operated with a Si (111) double crystal monochromator. During the measurement, the synchrotron was operated at 3.5 GeV and the current was between 150-210 mA. The data for each sample were collected three times and calibrated with standard Ti and Co metal foil. Data processing was performed using the program ATHENA.
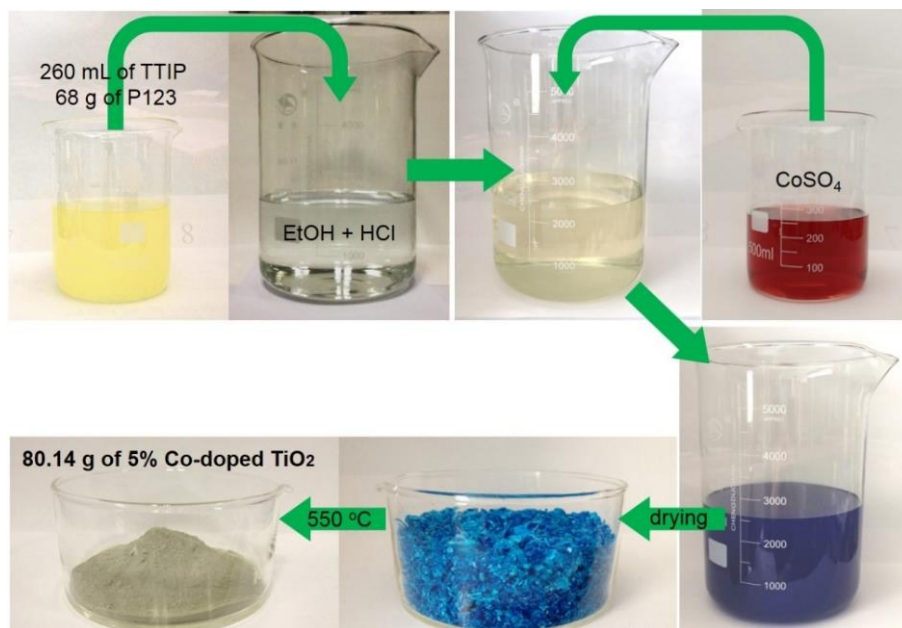
Fig. S1. Large-scale synthesis of Co-TiO$_2$ nanoparticles via sol-gel method. 80.14 g of 5 % Co-doped TiO$_2$ nanoparticles were finally obtained via sol-gel process in single batch.
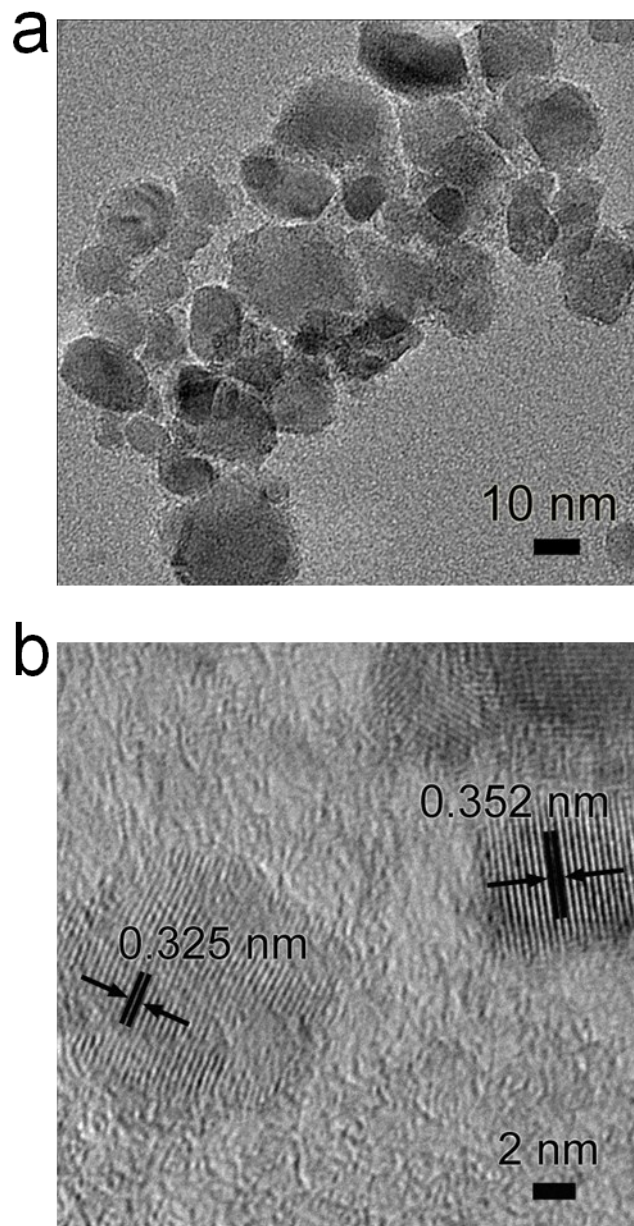
Fig. S2. Transmission electron microscopy (TEM) (a) and High resolution transmission electron microscopy (HRTEM) (b) images of pristine TiO_2 nanoparticles. TEM demonstrated that the diameter of as-synthesized pure TiO_2 nanoparticles was about 22 nm. HRTEM analysis suggested that pristine TiO_2 nanoparticles are of anatase phase (d=0.352 nm) and rutile phase (d=0.352 nm).
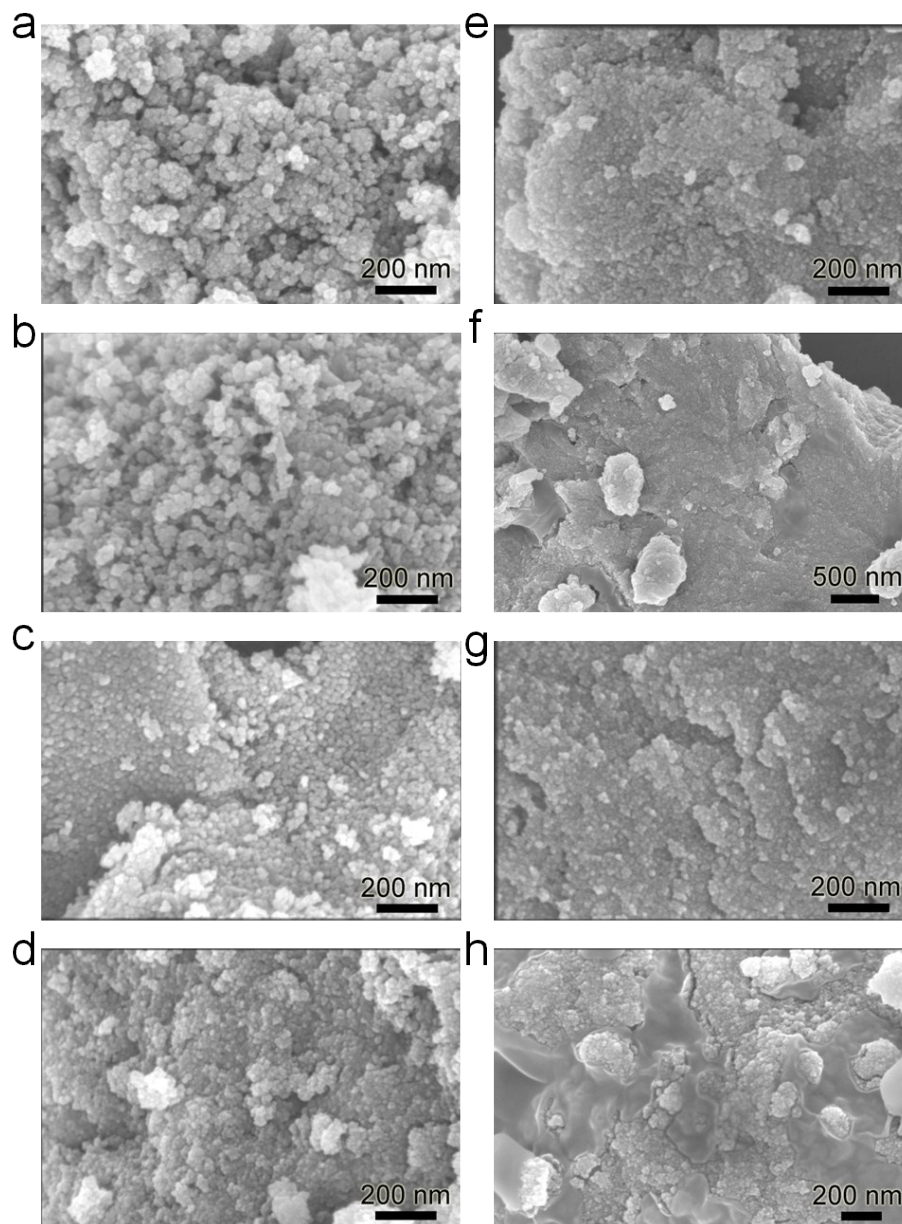
Fig. S3. SEM images of (a) pristine TiO_2 nanoparticles and Co-doped TiO_2 nanoparticles with the different amount of Co dopants: (b) 1 %, (c) 2.5 %, (d) 5 %, (e) and (f) 7.5 %, (g) and (h) 10 %. The particle size and morphology can be regulated by controlling the doping concentration.
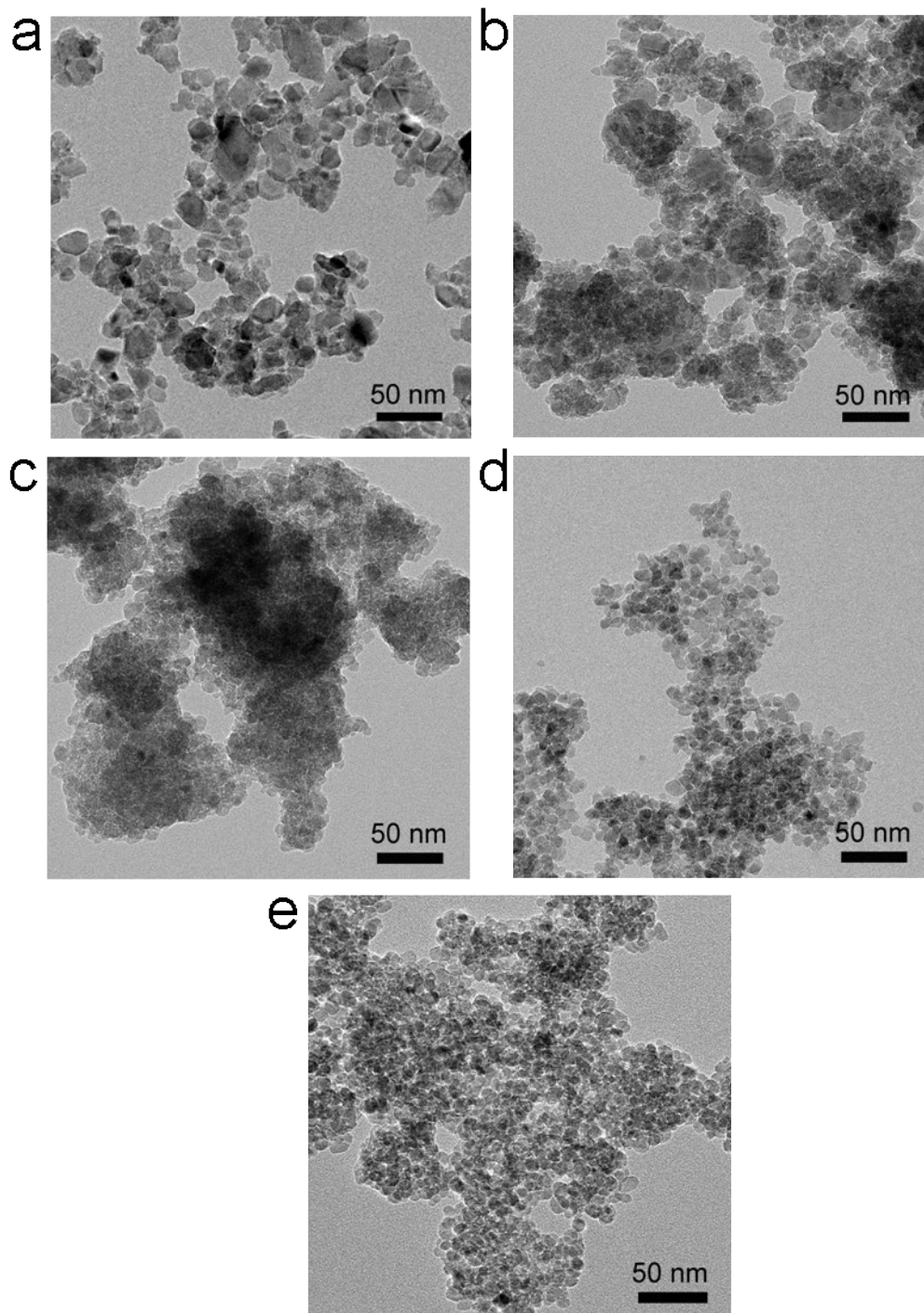
Fig. S4. TEM images of (a) pristine TiO_2 nanoparticles and Co-doped TiO_2 nanoparticles with the different amount of Co dopants: (b) 1 %, (c) 2.5 %, (d) 5 %, (e) 7.5 %.
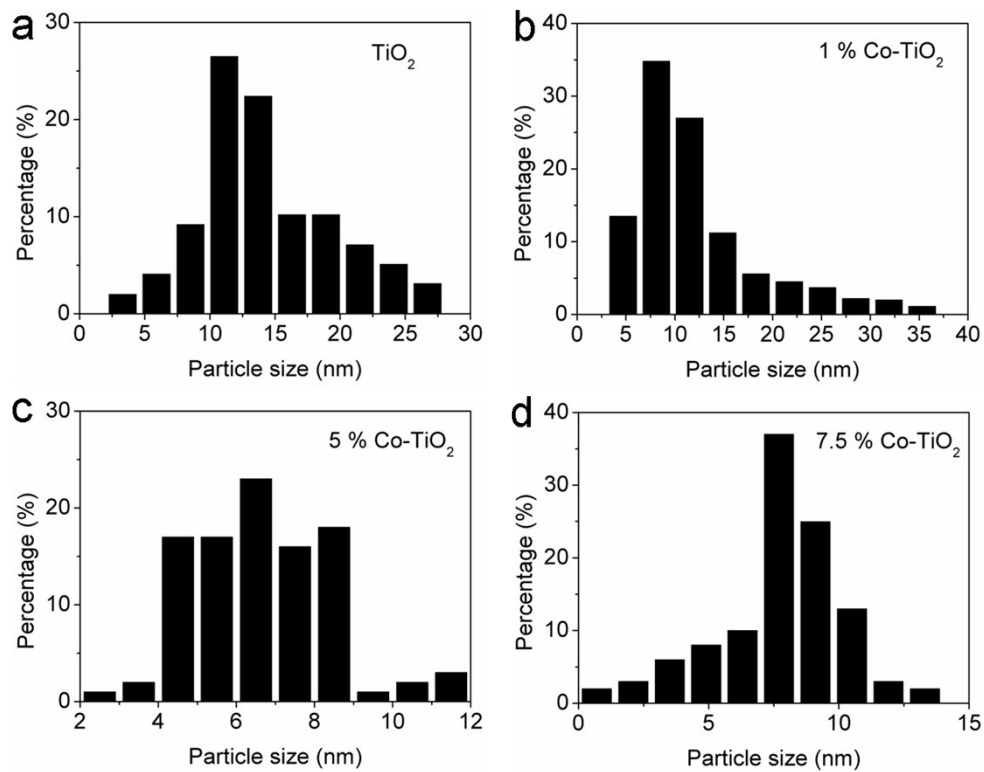
Fig. S5. Size distribution histograms calculated from the measured sizes of TiO_2 nanoparticles and Co-doped TiO_2 nanoparticles as derived from the TEM particle analysis.
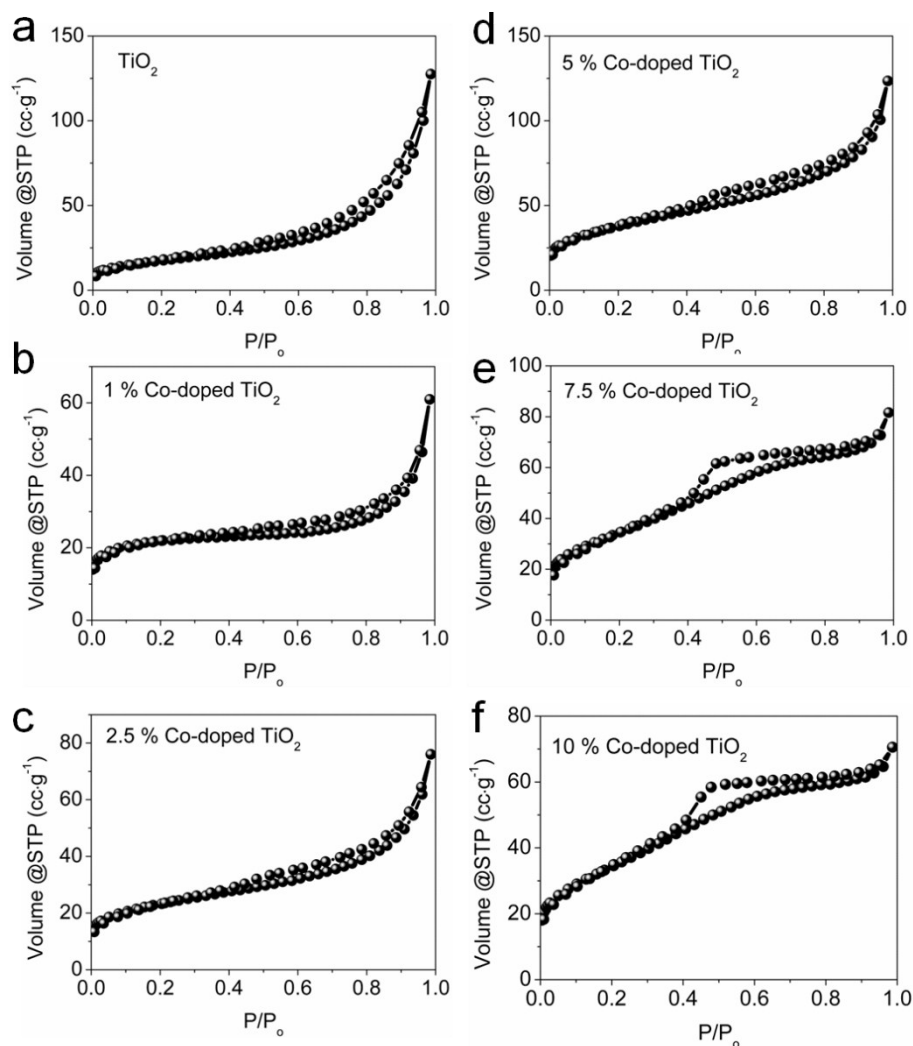
Fig. S6. N_2 adsorption/desorption isotherms of pristine TiO_2 and Co-doped TiO_2 nanoparticles. The surface area of TiO_2 and Co-doped TiO_2 nanoparticles were demonstrated by the N_2 adsorption-desorption analysis results. All the samples exhibit type IV isotherm curves with clear hysteresis loops, which are caused by significant agglomeration during high temperature calcinations process. By increasing the amount of doped Co, the specific surface area is first increased and then decreased. As shown in Table S1, the 5 % Co-doped TiO_2 nanoparticles exhibits the highest specific surface area of 130.3 $m^2 \cdot g^{-1}$.
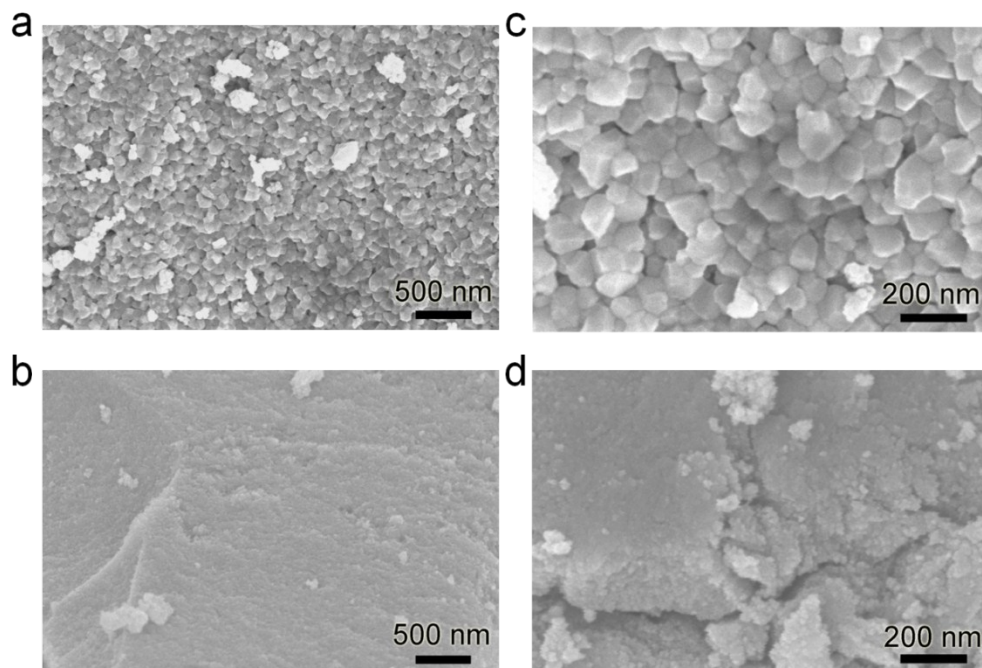
Fig. S7. SEM images of TiO$_2$ nanoparticles (a) and (c), and Co-doped TiO$_2$ nanoparticles (b) and (d) without the presence of P123. Larger pristine particles formed without the stabilization of P123. Small particle size of Co-doped TiO$_2$ sample again suggesting the roles of P123 and Co^{2+} ions as stabilizers.
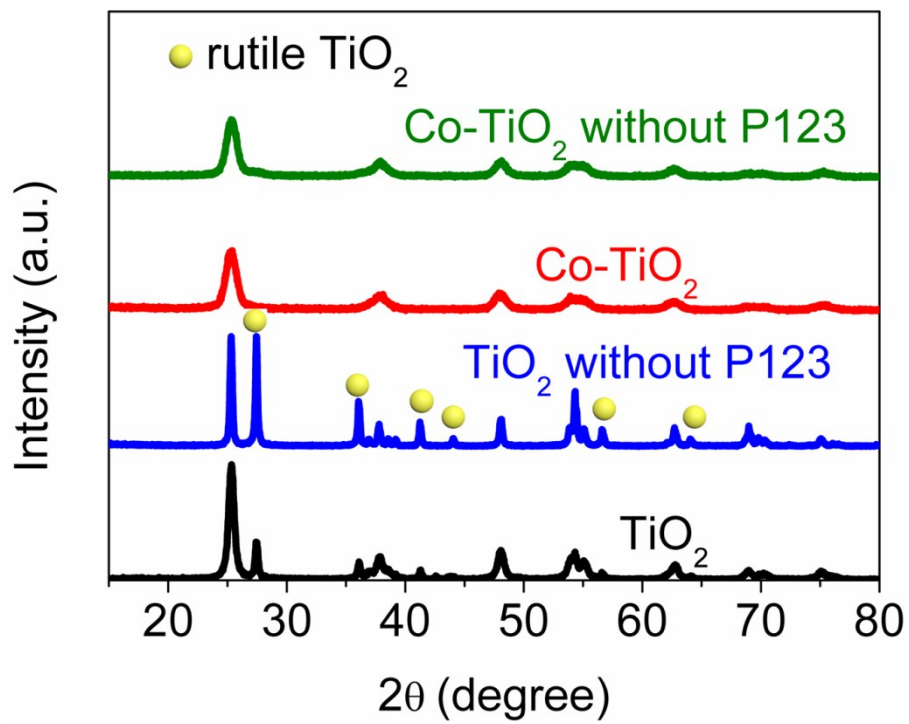
Fig. S8. XRD of TiO_2 nanoparticles and Co-doped TiO_2 nanoparticles obtained with and without the help of P123.
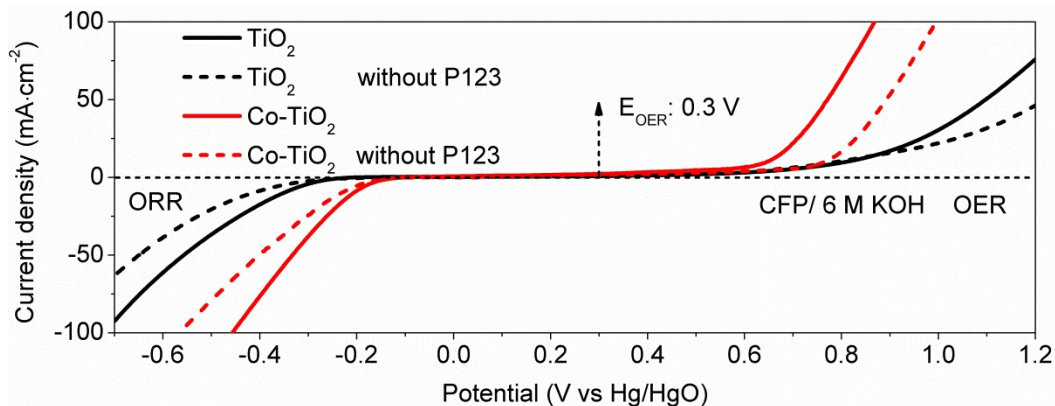
Fig. S9. Linear-sweep voltammograms (LSV) of TiO_2 and Co-doped TiO_2 nanoparticles in O_2-saturated 6 M KOH solution at scan rate of 10 mV·s^{-1}. TiO_2 nanoparticles without P123 for preparing exhibit poor ORR and OER activity due to the increased particle size and induced the density of active sites exposed to electrochemical interface. Compared with 5 % Co-doped TiO_2 that use P123 as surfactant, the nanoparticles without P123 for preparing exhibit poor ORR and OER activity due to particles aggregation which inhibit the transformation of O_2 and induce the O_2 reduction and evolution efficiencies.
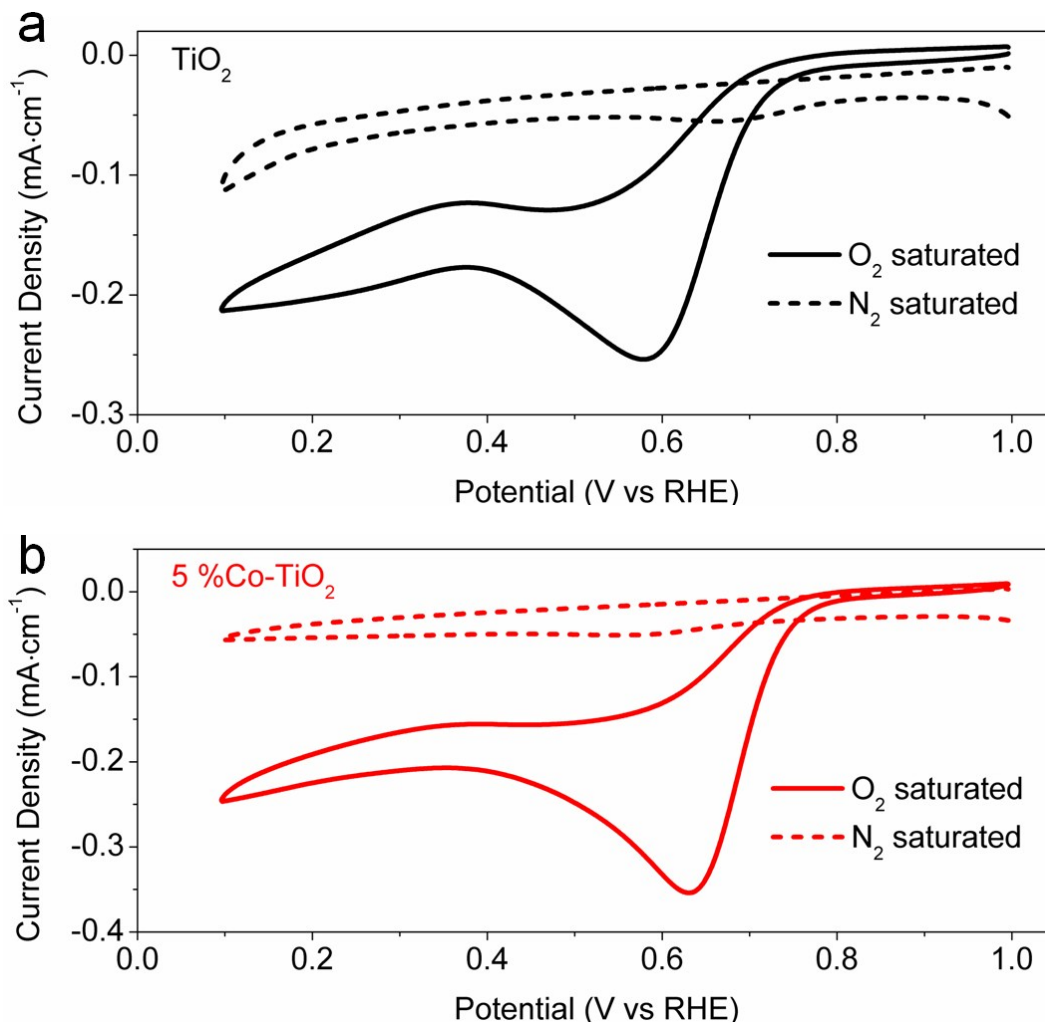
Fig. S10. CV curves of TiO_2 (a) and 5 % Co-doped TiO_2 on RDE (catalyst loading: 0.1 mg·cm^{-2}) in O_2-saturated (solid line) and N_2-saturated (dash line) 0.1 M KOH at a scan rate of 10 mV·s^{-1}.
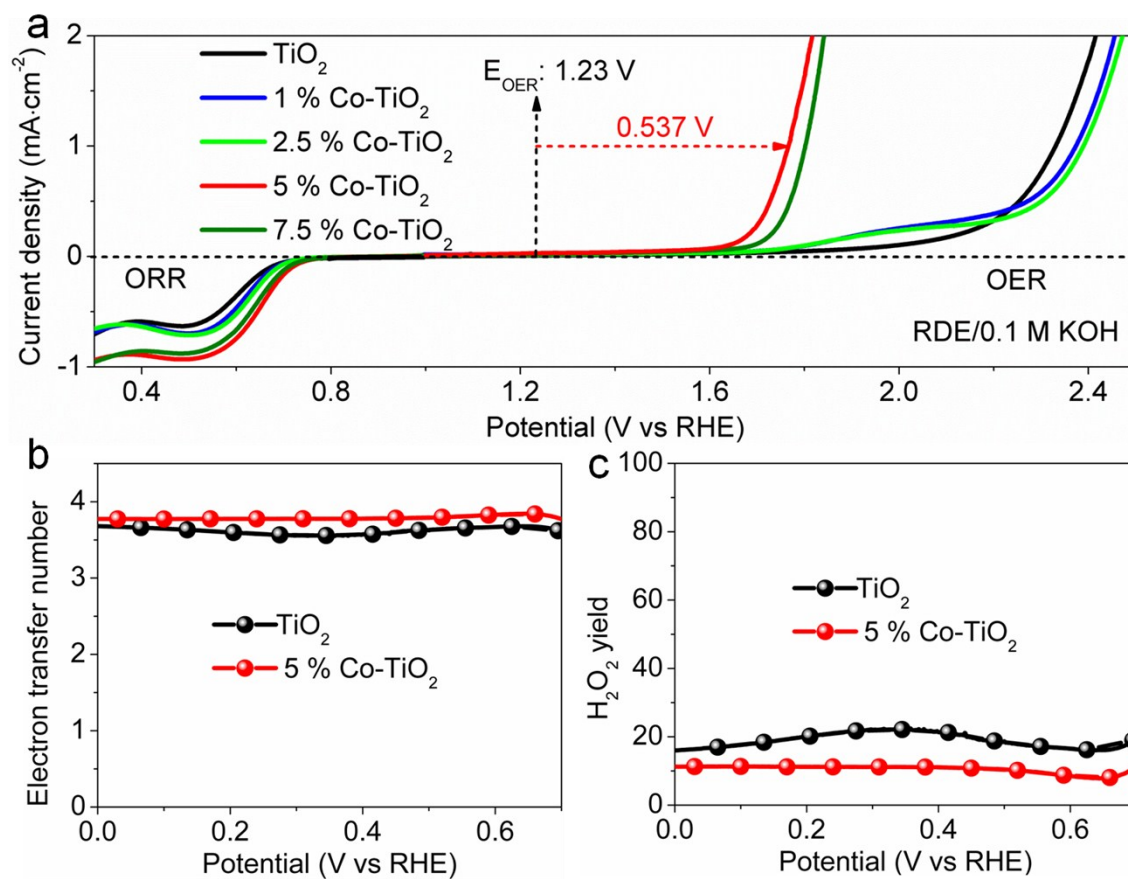
Fig. S11. ORR and OER polarization curves (a), electron transfer number (b) of various catalysts on RDE in 0.1 M KOH at a scan rate of 10 mV·s^{-1}. (c) RRDE polarization curves and peroxide yield of TiO$_2$ and 5 % Co^{2+}-doped TiO$_2$ in O$_2$-saturated 0.1 M KOH.The loading was 0.2 mg·cm^{-2} for all materials.
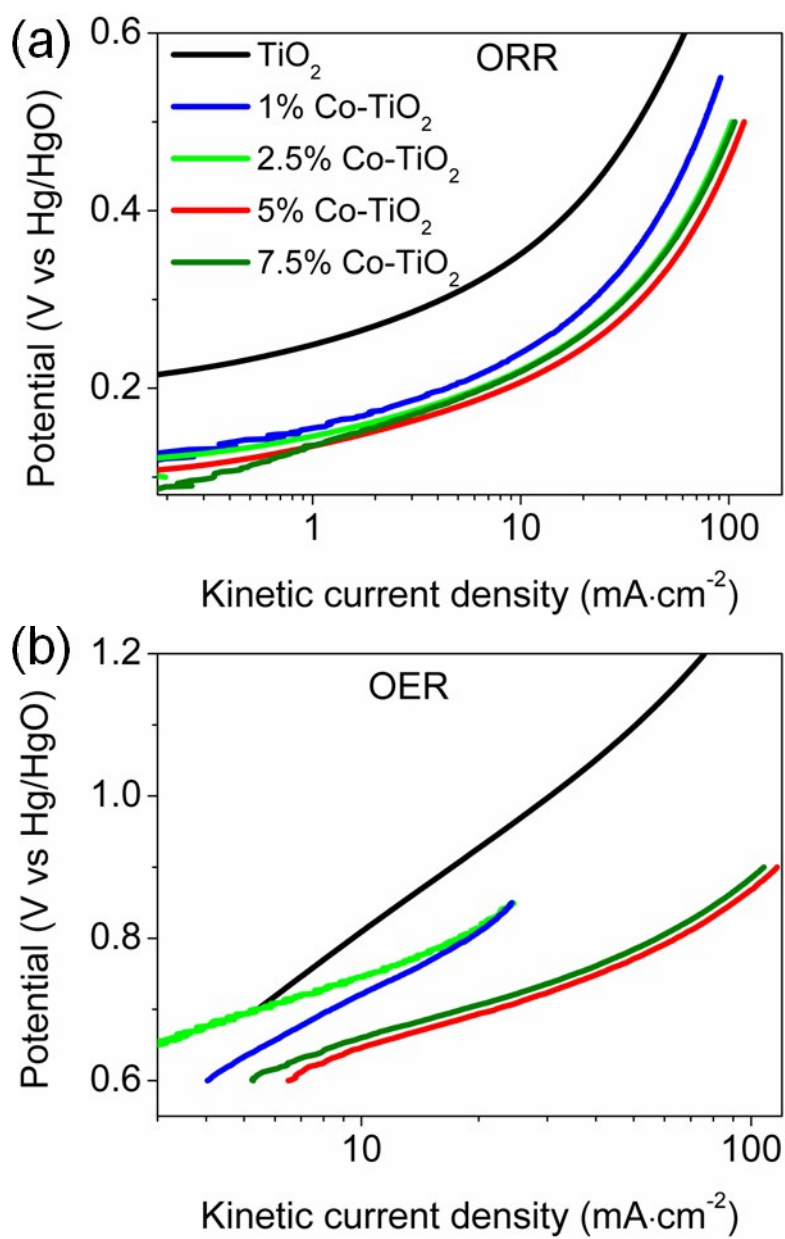
Fig. S12. The diffusion-current-corrected Tafel plots of TiO$_2$ and Co-doped TiO$_2$ nanoparticles for ORR (a) and OER (b).
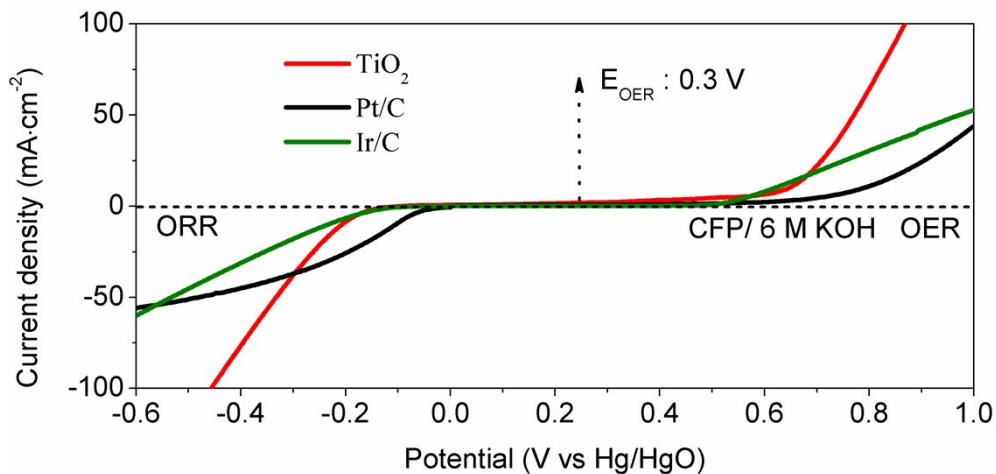
Fig. S13. ORR and OER polarization curves of 5 % Co-doped TiO_2 nanoparticles, Pt/C and Ir/C on Teflon-coated carbon fiber paper (CFP) electrodes in 6 M KOH. The catalyst loading on CFP electrodes was 2 mg·cm^{-2} for all materials.
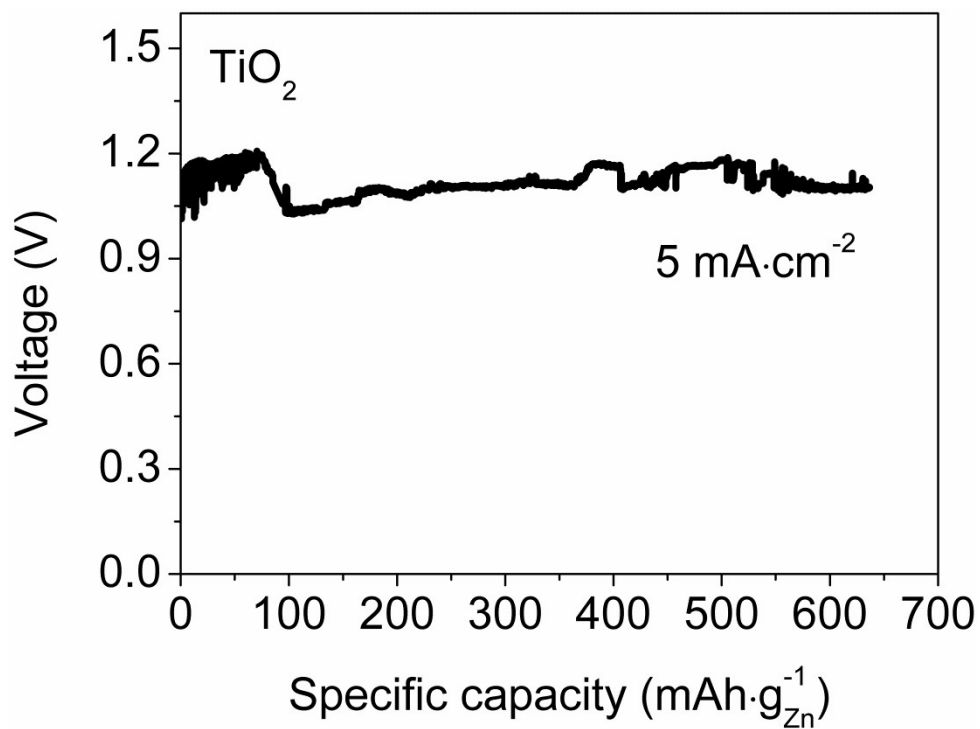
Fig. S14. Specific capacities of the Zn-air batteries using TiO_2 nanoparticles as ORR catalyst are normalized to the mass of the consumed Zn at current densities of 5 mA·cm^{-2}. When normalized to the mass of consumed Zn foil, the specific capacity of our battery based on TiO_2 nanoparticles electrocatalysts was 636.6 mAh·g_{Zn}^{-1} (corresponding to an energy density of 713.4 Wh·Kg_{Zn}^{-1}) at a current density of 5 mA·cm^{-2}.
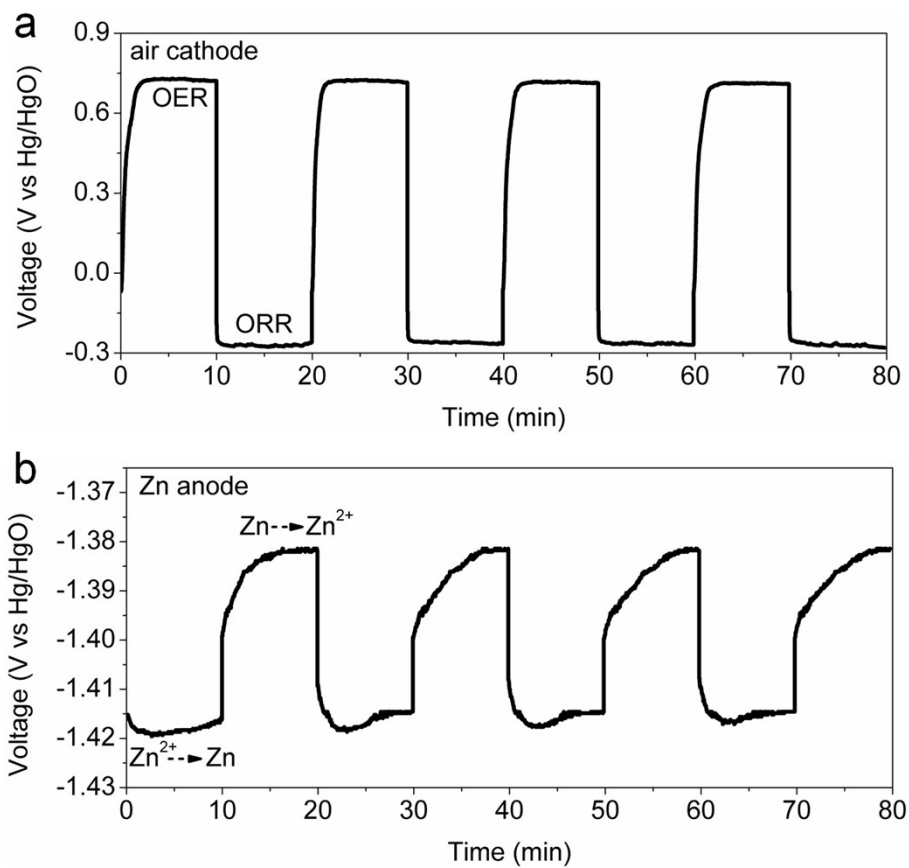
Fig. S15. Alternating oxidation and reduction of (a) the air cathode and (b) the Zn anode at a current density of 10 mA·cm^{-2}. Based on above data, the voltage polarization observed in Fig. 5b of the main text was mainly contributed by the air cathode side (sum of ORR and OER overpotentials). Polarization on the Zn anode was negligible.
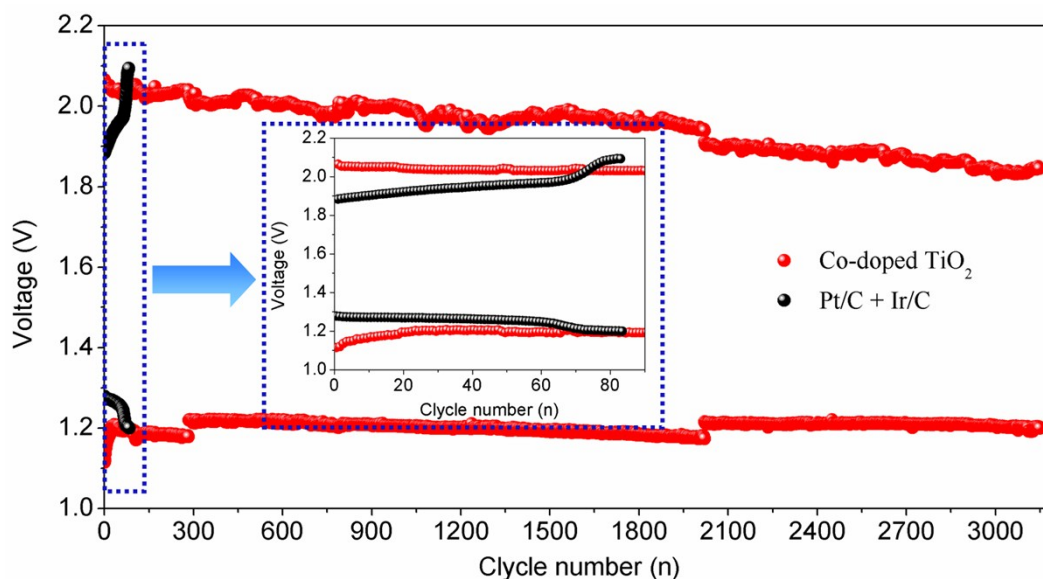
Fig. S16. Discharge/charge cycling curves of two-electrode Zn-air batteries made of Pt/C+Ir/C air cathode. The mass ratio of Pt/C and Ir/C is 1:1 with a total loading of 2 mg·cm^{-2} on CFP. The as-formed Zn-air battery was run at 5 mA·cm^{-2} in a short cycle period (1200 s per cycle) in 6 M KOH. At the first cycle, the charge-discharge voltage gap of Pt/C+Ir/C electrode (0.6 V at 5 mA·cm^{-2}) smaller than Co-doped TiO$_2$ electrode (0.94 V at 5 mA·cm^{-2}) because of the ORR and OER activity of the Co-doped TiO$_2$ are much inferior to that of Pt/C+Ir/C under 6 M KOH (Figure S13). After dozens of charge-discharge cycles, the charge-discharge voltage gap of Co-doped TiO$_2$ electrode was similar with Pt/C+Ir/C electrode. On the one hand, the charge-discharge voltage gap of Pt/C+Ir/C electrode became broader after multiple charging-discharging cycles reached to 0.90 V after 80 cycles (Figure S16), suggesting the poor stability of air electrode based on Pt/C+Ir/C electrocatalyst. On the other hand, the potential gap of Co-doped TiO$_2$ electrode is gradually decreasing along with the discharge/charge cycle number, presumably due to further activation of the Co-doped TiO$_2$ electrode material by the basic electrolyte. Detailed investigation on such a promoting effect of recycling test was also in progress in our lab.
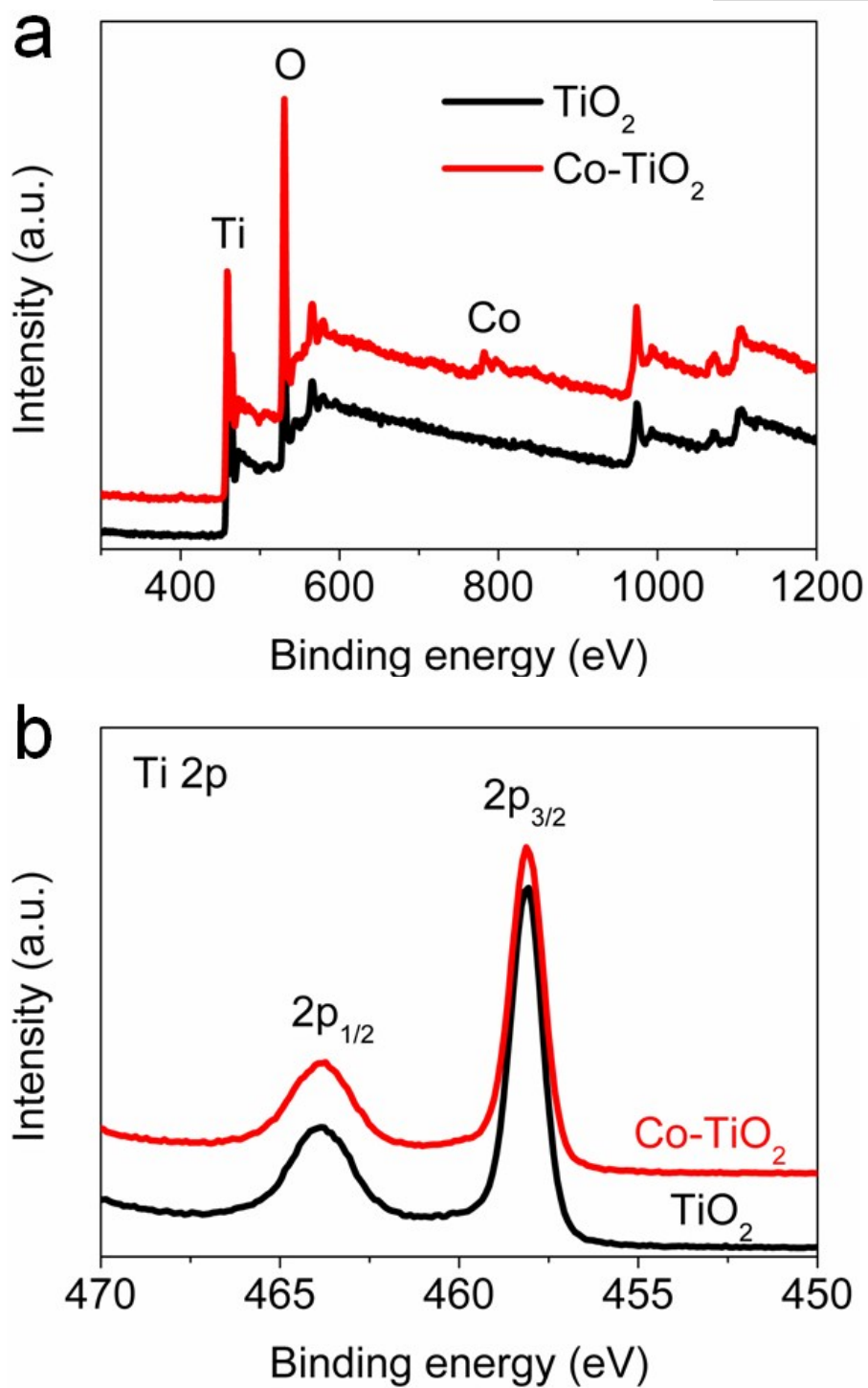
Fig. S17. XPS survey spectra (a) and high-resolution XPS Ti 2p spectra (b) of pristine TiO_2 and 5 % Co-doped TiO_2 nanoparticles.
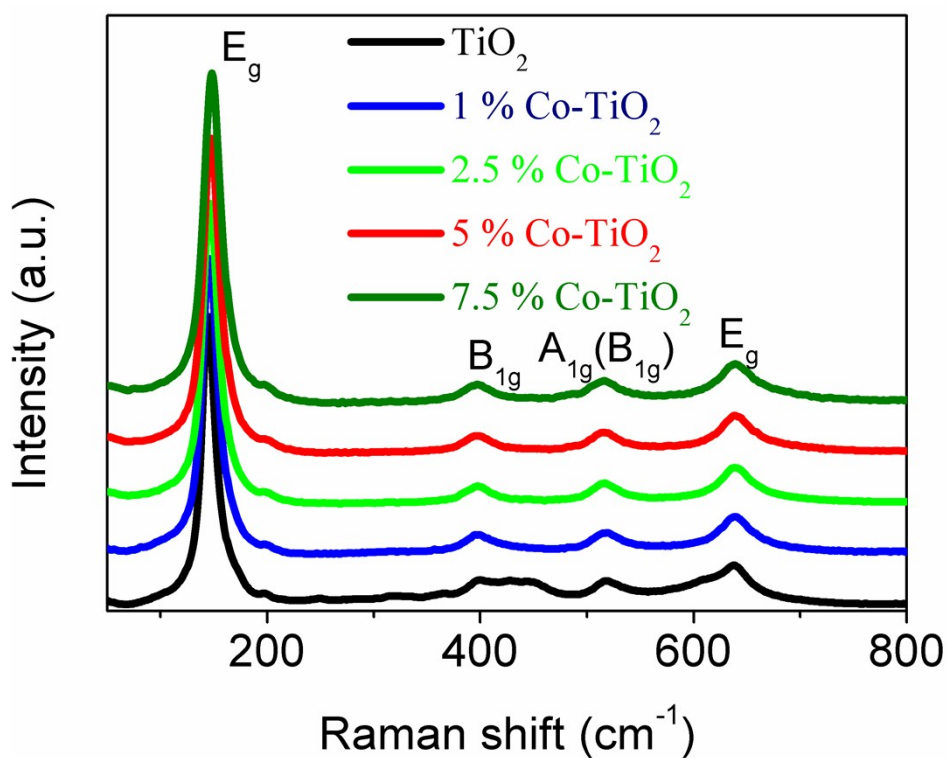
Fig. S18. Raman spectra of pristine TiO_2 and Co-doped TiO_2 nanoparticles. All six active Raman modes (A_{1g}, B_{1g} and E_g) in anatase TiO_2 are assigned. The prominent Raman scatterings at 141, 198, 397, 514, and 637 cm^{-1} are assigned as Eg, B_{1g}, B_{1g} + A_{1g}, and Eg, respectively. The Raman peak at 141 cm^{-1} is due to the symmetric stretching of Ti-O-Ti bonds whereas peaks at 397 and 514 cm^{-1} are due to symmetric and antisymmetric bending vibrations, respectively.

Table S1. Surface area of TiO_2 and Co-TiO_2 nanoparticles.

Sample	surface area BET ($m^2 \cdot g^{-1}$)
TiO_2	62
1 % Co- TiO_2	64.24
2.5 % Co- TiO_2	75.9
5 % Co- TiO_2	130.3
7.5 % Co- TiO_2	124
10 % Co- TiO_2	123.8

.

Table S2. The atomic contents of Co, Ti, O in TiO$_2$ and Co-TiO$_2$ nanoparticles according to the XPS reports.

Sample	O /atom %	Ti /atom %	Co /atom %	Co/(Co+Ti) /%
TiO$_2$ nanoparticles	69.62	30.38	0	0
Co-TiO$_2$ nanoparticles	71.21	25.84	2.95	10.2

And contents of Co is 2.95 at.% (the atom ratio of Co/ (Ti+Co) is 10.2 %), which is larger than theoretical value. This may be that most of Co^{2+} largely substitutes for the Ti^{4+} sites and creat more acticity sites on the surface of TiO$_2$ lattice. There is a consensus that the Co-doped TiO$_2$ nanoparticles would benefit their potential applications as electrocatalysts via enriching active centers.

Table S3. Performance of TiO_2 and Co-TiO_2 nanoparticles and state-of-the-art rechargeable Zn-air batteries in the literature.

Electrocatalysts	Peak power density ($mW\cdot cm^{-2}$)	Specific capacity ($Wh\cdot Kg^{-1}_{Zn}$)	Ref
Co-doped TiO_2	136	938.5	This work
2DBN-800	23.9	_	S1
CuFe alloy catalyst	212	_	S2
Cu-Pt Nanocage	_	728	S3
rGO-IL	120	_	S4
nitrogen-doped carbon nanofiber	_	760	S5
Carbon black/manganese oxide	67.51	798 ± 20	S6
Ni modified MnO_x/C composites	122	_	S7
Graphene-Supported $CoMn_2O_4$	_	610	S8
Fe@N-C	220	_	S9
NPMC-1000	55	835	S10
$LaCoO_3$	77	_	S11

Table S4. Rechargeability of Co-TiO$_2$-based two-electrode Zn-air battery and state-of-the-art rechargeable Zn-air batteries in the literature.

Configuration	Electrocatalysts	Voltage polarization	Cycle number	Ref
Two-electrode	Co-doped TiO$_2$	0.81 V at 5 mA/cm^2	1200 s/cycle for 3150 cycles (**1050 h**)	This work
		1.0 V at 20 mA/cm^2	20 h/cycles for 37 cycles (750 h)	
	2DBN-800	～1.3 at 5 mA/cm^2	300 s/cycle for 11h	S1
	Graphene-CoMn$_2$O$_4$	0.95V at 20 mA/cm^2	600 s/cycle for 200 cycles	S9
	Fe@N-C	～1.2 V at 1 mA/cm^2	1 h/cycle for 100 cycles	S10
	MnO$_2$-NCNT	1.5 at 20 mA/cm^2	600 s /cycle for 50 cycles	S13
	NPMC-1000	～1.26 V 5 mA/cm^2	600 s/cycle for 180 cycles (30 h)	S11
Tri-electrode	NPMC-1000	～1.26 V 5 mA/cm^2	600 s/cycle for 600 cycles (100 h)	S11
	LaCoO$_3$	0.99V at 10 mA/cm^2	300 s/cycle for 150 cycles	S12

Supplementary References

[S1]   X. D. Zhuang, D. Gehrig, N. Forler, H. W. Liang, M. Wagner, M. R. Hansen, F. Laquai, F. Zhang and X. L. Feng, *Adv. Mater.,* 2015, **27**, 3789-3796.

[S2]   G. Nam, J. Park, M. Choi, P. Oh, S. Park, M. G. Kim, N. Park, J. Cho and J-S. Lee, *ACS nano.,* **2015**, **9**, 6493-6501.

[S3]   V. M. Dhavale and S. Kurungot, *ACS Catal,.* 2015, **5**, 1445-1452.

[S4]   J. S. Lee, T. Lee, H. K. Song, J. Cho and B. S. Kim, *Energy Environ. Sci.,* 2011, **4**, 4148-4154.

[S5]   H. W. Liang, Z. Y. Wu, L. F. Chen, C. Li and S. H. Yun, *Nano Energy,* 2015,**11**, 366-376.

[S6]   P. C. Li, C. C. Hu, T. C. Lee, W. S. Chang and T. H. Wang, *J. Power Sources.,* 2014, **269**, 88-97.

[S7]   Q. M. Wu, L. H. Jiang, L. T. Qi, E. Wang and G. Q. Sun, *Int. J. hydrogen energy*., 2014, **39**, 3423-3432.

[S8]   J. Wang, H. H. Wu, D. F. Gao, S. Miao, G. X. Wang and X. H. Bao, *Nano Energy,* 2015, **13**, 387-396.

[S9]   J. T. Zhang, Z. H. Zhao, Z. H. Xia and L. M. Dai, *Nature Nanotech.,* 2015, **10**, 444-453.

[S10]   C. Y. Zhu, A. Nobuta, I. Nakatsugawa and T. Akiyama, *Int. J. hydrogen energy*., 2013, **38**, 13238-13248.

[S11]   M. Prabu, P. Ramakrishnan, H. Nara, T. Momma, T. Osaka and S. Shanmugam, *ACS Appl. Mater. Interfaces,* 2014, **6**, 16545-16555.

[S12]   Z. Chen, A. P. Yu, R. H. Ahmed, H. J. Wang, H. Li and Z. W. Chen, *Electrochim. Acta.,* 2012, **69**, 295-300.